Demonstration of the Shock-Timing Technique for Ignition Targets at the National Ignition Facility

Introduction

Ignition experiments at the National Ignition Facility (NIF) will use x rays in indirect-drive (hohlraum) targets to drive implosions of capsules containing deuterium–tritium (DT) fuel.[1] These inertial confinement fusion (ICF) targets use three shock waves to quasi-isentropically compress the capsule before the main compression wave drives the implosion of the fuel assembly.[2] The goal is to minimize the required drive energy by minimizing the entropy imparted to the capsule as it is imploded. To achieve ignition, both the strength and timing of the shock and compression waves must be accurately set.

The National Ignition Campaign (NIC) is a multi-laboratory program[3] that designed and will perform experiments that lead to ignition on the NIF. The campaign includes various tuning experiments that iteratively optimize the laser and target parameters to achieve specified conditions and maximize target performance. To achieve optimal shock conditions, experiments using optical diagnostics will detect the shock-velocity temporal profiles, providing both the strength and timing of the various shocks within the capsule fuel.[4] The tuning campaign will use these data to adjust the laser (and, therefore, x-ray) drive until the shock strengths and timings meet design specifications. These experiments require surrogate targets that make it possible to diagnostically access the inside of the capsule but closely mimic the behavior of the ignition targets. The ignition capsule in these targets has a re-entrant Au cone filled with liquid deuterium and extends out beyond the hohlraum wall.[5] With these targets, optical diagnostics can detect spherically converging shock waves within the deuterium-filled capsule.

Optical diagnostics can readily measure both shock velocity and timing to the precision and accuracy required for ignition target designs. These measurements, taken in a cryogenic capsule embedded in a hohlraum and driven to radiation temperatures in excess of 150 eV, present considerable challenges. To demonstrate that this is a viable technique for the NIF, experiments were performed at the Omega Laser Facility.[6] This article discusses the resolution of several issues associated with this approach and demonstrates that this technique is a valid method to time shocks in ignition targets on the NIF.

Shock Timing

ICF targets are spherical shells that have a layer of solid (cryogenic) DT fuel that must be compressed to 1000 g/cc on a low adiabat and then heated to ~5 keV to initiate ignition and burn.[1] This compression is produced by the ablation process that can be driven either directly or indirectly by laser beams. In the indirect case, the capsule is contained in a cylindrical hohlraum that is irradiated by many high-power laser beams that produce up to a 1×10^{15} W/cm^2 flux of thermal x rays that drive an ablative implosion of the capsule. Target design is a delicate optimization of maximizing fuel compression while minimizing the internal energy imparted to the pusher and fuel. The primary approach is to approximate an isentropic compression using a series of three shock waves of increasing strength, followed by a compression wave that drives the compressed shell of fuel to implode at velocities of ~3.6×10^7 cm/s. Shock waves provide discrete "markers" that will be used to diagnose the compression history. The steps in drive pressure (that produce the shocks) are controllable parameters that make it possible for the compression to be optimized while controlling entropy increases. Shock waves are also desirable for ablators that may have a spatial structure that can be smoothed out by the melting produced by a first shock.[7]

In its simplest form, an ICF target is a two-layer system—an ablator surrounding a layer of DT ice. (Actual ablators have internal layers of varied composition to enhance the absorption and ablation processes.[8]) For optimal target performance each shock must have the correct strength. Specification requires that the velocity be set to a precision of 1%. The shocks must arrive at the inner DT-fuel surface in a tight sequence, with their launch times known to a precision of 50 ps (Ref. 4). The assembled mass is swept inward by the compression wave that must be timed to a precision of 100 ps. When properly tuned in strength and timing, the shocks minimize the adiabat (internal energy) of the DT fuel, keeping it on a low isentrope. By

arriving at the inner surface of the ice in a tightly controlled sequence, most of the fuel has been shocked and re-shocked along a low adiabat.

If the later, stronger shocks overtake the first shock too early, a large portion of the fuel is heated by this strong shock and will be on a higher adiabat and be harder to compress. Late coalescence means that previous shocks have time to unload significant material from the inner surface of the ice, creating a low-density blowoff that would be significantly heated by the subsequent shocks, again placing the fuel on a higher isentrope.

Temporal profiles of the laser and resultant radiation temperature need to produce the desired shock strengths and timing. The residual uncertainties in the calculated hohlraum drive and the opacity and equation of state (EOS) of the ablator and fuel require full-scale tuning experiments to achieve the precision required for ignition. The NIC includes experiments that will iteratively "fine tune" the drive to optimize shock timing. Critical to this effort are precise measurements of shock timing in surrogate targets that are equivalent to ignition targets.

Figure 117.1(a) depicts the Lagrangian trajectories of four shocks through the ablator and DT ice. For optimal performance, these shocks should arrive at the inner DT-ice surface in a tight temporal sequence.[4] The laser pulse shape for ignition targets is shown schematically in Fig. 117.1(b), along with the expected radiation temperature in the hohlraum. The steps in the radiation temperature launch three successive shocks with pressures of approximately 0.8, 4, and 12 Mb in the DT fuel. The main compression wave begins with pressures greater than 40 Mb. (Individual designs vary these values slightly.)

Since the EOS of deuterium is known,[9] a measurement of the shock velocity provides all the pertinent information about the shock wave. The NIC shock-timing campaign will use shock-velocity measurements to iteratively adjust the level and timing of each "step" in power to produce the desired shock velocity (pressure) and timing. Knowledge of the temporal velocity profiles provides, through integration, the positions of shock coalescence.

The velocity interferometry system for any reflector (VISAR)[10] probe beam is reflected off the leading shock front (the one closest to VISAR). At these pressures, shock-compressed deuterium is a metal-like reflector that is opaque to visible light.[11] The following shock fronts cannot be viewed inside the opaque medium; instead, they are detected only when they overtake or coalesce with the leading shock front.
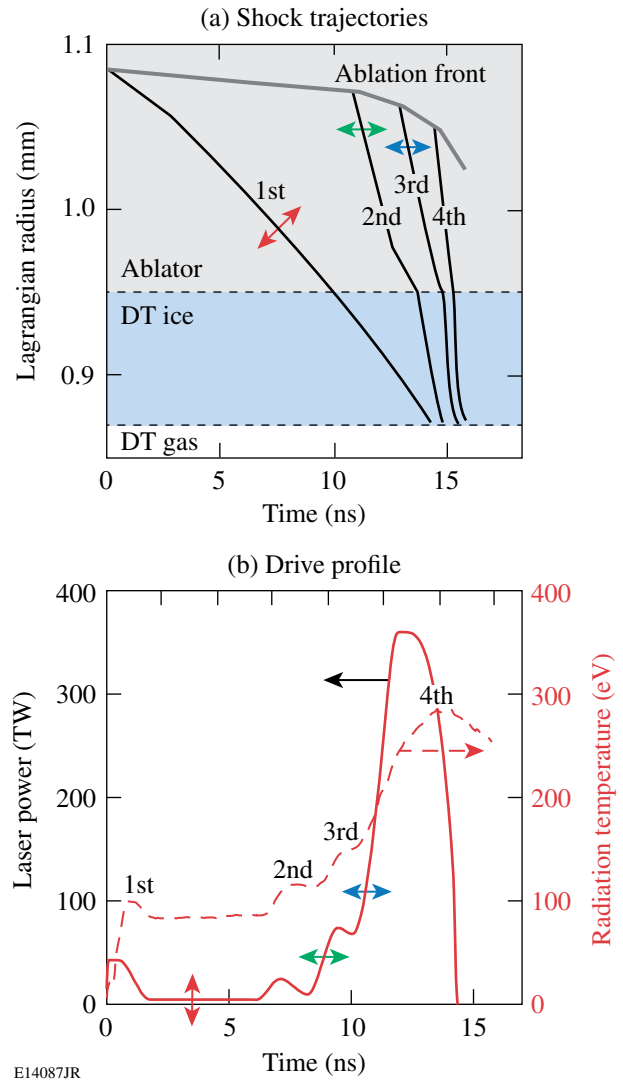
Figure 117.1

(a) Lagrangian trajectories of shocks in an ignition target showing optimal timing with shocks arriving at the inner DT-ice surface in a tight sequence. (b) Temporal history of laser intensity and resulting radiation temperature for an ignition target on the NIF. A shock-timing tuning campaign will iteratively adjust (arrows) the laser pulse shape to optimize shock timing.

The single-shock velocities corresponding to the pressures of the first three steps in the drive pulse (i.e., following coalescence) are approximately 20, 36, and 57 km/s, respectively. (Again, there are several designs and the specified velocities range by ~5% from those values, depending on how the implosion optimization is performed.) For a given design the velocity can have a 2% shot-to-shot variation, but to ensure proper timing, the shock velocities will be measured with a precision of 1% and the coalescence times to less than 30 ps. For the 75-μm-thick DT layer the transit time of the first shock is

~3.75 ns. By integrating the first shock velocity (known to 1%) up to the coalescence time (known to 30 ps), one can determine the coalescence position to a precision of <2 μm. The precision of the VISAR diagnostic is more than adequate to determine this position. The error budget for shock-strength and timing experiments is readily met if the velocity is measured to 1% and shock timing is measured to 30 ps.

A DT ignition capsule has a specific drive profile needed to achieve optimal performance. To guide the ignition-tuning campaign, that optimal drive profile is applied (in simulations) to a capsule containing liquid deuterium–deuterium (DD). The resultant shock structure (velocity profiles and timing) in that simulation then serves as the metric to which shock-timing experiments are gauged. The optimal shock strengths (velocities) in liquid DD are obtained from this simulation. Because the shock velocities (but not the shock pressures) are nearly the same in liquid DD as in solid DT, the optimal coalescence position for the shock-timing experiments is very close to that in the solid-DT layer of an ignition capsule. This simulation procedure introduces a surrogacy error that is estimated to be less than 1% in shock velocity.

Experimental Technique

1. VISAR Windows

VISAR has been extensively used to detect and measure laser-driven shock waves in transparent media and has a demonstrated shock-speed precision of 1%–2% and temporal accuracy of <30 ps (Refs. 12–14). Shock waves with pressures above ~0.2 Mb transform liquid deuterium (normally transparent) into a conducting medium;[11] as a result, the steep shock front (a conducting surface) readily reflects the VISAR probe beam at a wavelength of 532 nm (and similarly at 590 nm for the NIF VISAR). The arms of a VISAR interferometer have unequal optical paths and produce an output phase that is proportional to the Doppler shift of the reflected probe beam and to the difference in the unequal paths (usually expressed as a time delay). The time delay determines the velocity sensitivity of the interferometer and is adjustable (proportional to the thickness of a glass delay element placed in one arm of the interferometer). For these experiments, the VISAR on OMEGA had a velocity error of ~1.7%. The NIF VISAR is designed to achieve 1% velocity measurements.

Cryogenic targets require a closed volume to retain the deuterium gas. In a standard target, the spherical shell is the boundary of that volume. In shock-timing experiments a line of sight is needed for VISAR to probe the shock-velocity profile. Various target configurations were considered, but the stringent

performance tolerances dictated that shock-timing surrogate targets mimic ignition targets with high fidelity. For the NIC tuning experiments, spherical targets will be fitted with a re-entrant cone that extends through the hohlraum wall and is capped by a 20-μm-thick quartz window that confines the DD fuel. This target configuration is shown in Fig. 117.2. Integrated 3-D simulations of this target show that perturbations to the radiation temperature and hohlraum symmetry are minimal.[15] By design, the change in the albedo caused by the portion of the cone traversing the hohlraum-capsule space is offset by that of the sections of ablator surface and hohlraum wall displaced by that cone. It is expected that on the hohlraum wall, where shock timing is measured, the radiation flux will mimic a full ignition target to ~4% (1% in T_{rad}) (Ref. 5).

It has been shown that for direct-drive targets at high intensities the normally transparent material ahead of the shock wave can absorb the VISAR probe laser.[16] This is caused by high-energy x rays produced in the laser-plasma corona.[17] The x rays photoionize the unshocked material, creating free electrons that interact with and absorb the probe light, causing a "blanking" of the probe beam in the material. This could compromise the VISAR data. This is not expected to be a problem in the deuterium (which has a low x-ray-absorption cross section), but the diagnostic window that retains the DD

Hard x rays from laser spots can blank diagnostic window

Capsule

D_2

Diagnostic window

E15108JR
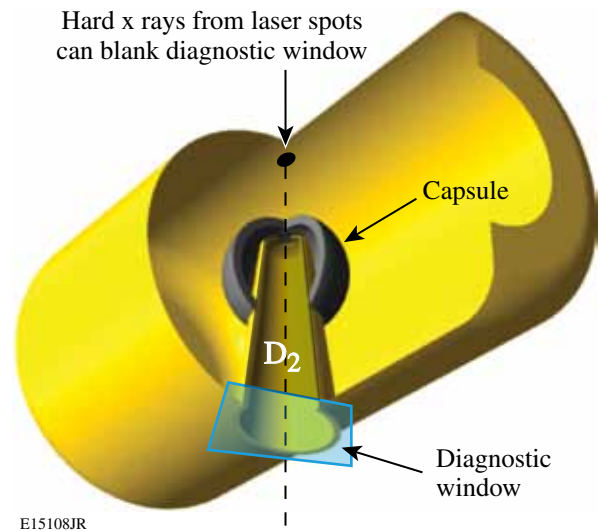
Figure 117.2
NIC shock-timing tuning experiments will use ignition-style targets that have a re-entrant cone in the capsule. The capsule and cone are filled with liquid deuterium. Optical diagnostics probe the inside of the capsule through the window and aperture in the cone.

in the NIF shock-timing targets (Fig. 117.2) can experience this ionization blanking.

Single-sided [one laser entry hole (LEH)] hohlraum experiments with cryogenic and warm targets were used to study this effect and to select a window material. Windows made of silicon nitride, diamond, sapphire, and quartz were tested. Quartz (20 μm thick) was chosen because of its resistance to blanking (band gap of ~15 eV), optical quality, and ease of fabrication. Though quite resilient, quartz, nevertheless, blanks if exposed to sufficient x-ray flux.

In NIF shock-timing targets, the VISAR window has a line of sight through the ablator material to the hohlraum wall that is directly irradiated by laser beams (Fig. 117.2). Since the ablator absorbs most of the radiation below ~1.5 keV, ionization blanking in these targets results primarily from the Au M-band (2 to 4 keV) emission produced by the laser spots. The VISAR cone has a 260-μm hole at the end through which shock timing is measured. The aperture size has been chosen to limit the extent of the hohlraum wall with a "view" of the VISAR window without limiting the area over which a VISAR signal can be collected for NIC-scale capsules. Figure 117.3(a) is a map of beam placement on the interior of a NIF ignition hohlraum. While the capsule is driven by *thermal* radiation from many beams, the VISAR window is irradiated by M-band emission ($h\nu > 2$ keV) that originates only from beam spots in the line of sight through the cone aperture. The region on the hohlraum wall that can irradiate the VISAR window is shown as the black dot in Fig. 117.3(a). Two NIF quad beam spots overlap at that point.

A series of experiments were performed on the OMEGA laser using planar targets to investigate the effect of x-ray emission from laser spots on the optical transmission of quartz windows. The configuration is shown in Fig. 117.3(b). A gold foil was placed 1.5 mm from a Be−Cu−Be sandwich (75, 0.5, and 75 μm thick, respectively) that mimics the opacity of a typical NIC ablator design. An aperture was placed directly behind the ablator and a window was placed 3.5 mm from the Au foil. VISAR probed the rear surface of the aperture and ablator (through the aperture). Nine OMEGA beams without beam smoothing were focused onto the gold foil to replicate the wall intensity of a NIF target at the relevant incidence angle (60°). The window transmission was observed, and the intensity at which x rays from the laser spots would blank the window was determined. The energy and pulse widths available on OMEGA dictate that the test be done in two steps,
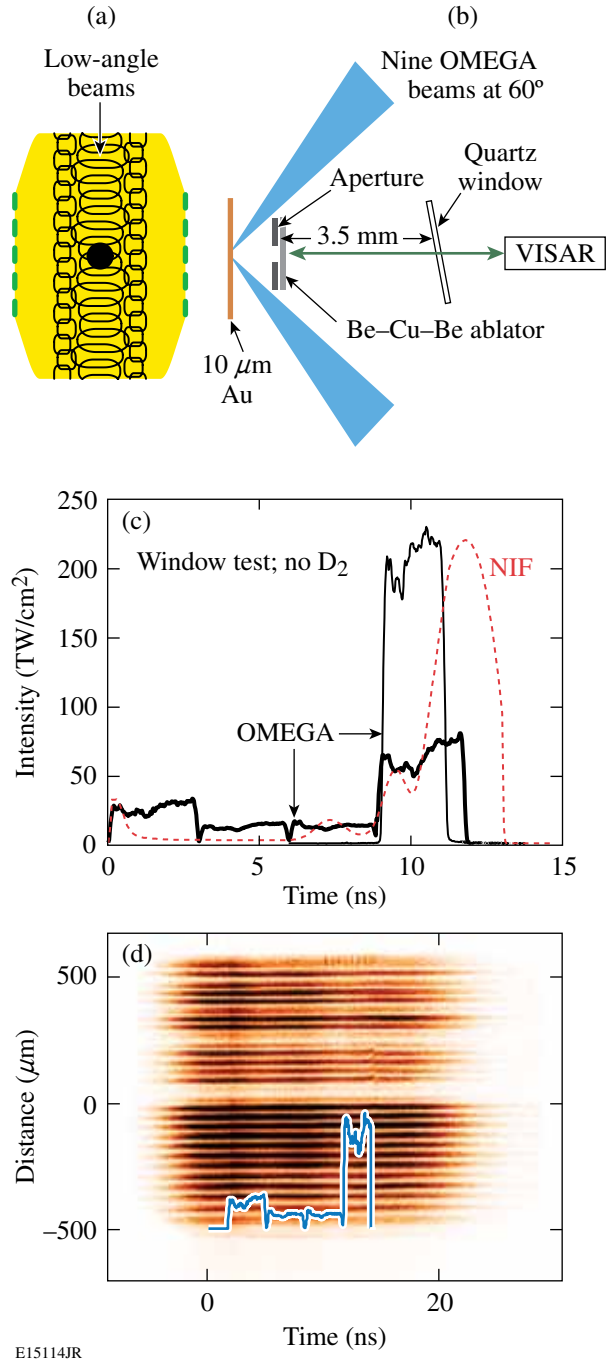
Figure 117.3
(a) The pattern of beam spots in an ignition hohlraum. (b) Target configuration to study effects of M-band emission on windows. (c) NIF laser intensity at the hohlraum equator wall (dashed curve); laser intensity for OMEGA experiments with stacked pulses (solid curves). (d) VISAR data from a stacked-pulse OMEGA experiment showing continuous fringes. The quartz window remains transparent throughout irradiation history, indicating that M-band emission from the laser spot does not "blank" (photoionize) the quartz.

separately measuring peak and integrated fluences associated with ignition-target conditions up to the breakout time of the third shock. Figure 117.3(c) (dashed curve) shows the incident intensity at the NIF hohlraum wall at the VISAR window line of sight [Fig. 117.3(a)]. The intensity profile for the OMEGA experiment with nine beams having temporally square pulses staggered to approximate the NIF wall intensity up to 12 ns is also shown (thick curve). Figure 117.3(d) shows a VISAR record with fringes that have continuous intensity throughout that experiment, indicating that the window remains transparent. Similar results were obtained for nine beams overlapped [thin solid curve in Fig. 117.3(c)] to replicate the intensity at the fourth rise. To investigate the limiting flux for this configuration, a third experiment was performed with a 1-ns pulse at 500 TW cm^2. At this fluence the quartz window blanked, but this is 2.5× higher than required for the NIF.

These results indicate that the quartz windows remained transparent when exposed to both the instantaneous flux and the integrated flux (up to the third shock) required for shock timing. These tests are conservative in that the NIF beams have high angles of incidence and will traverse considerable plasma en route to the hohlraum wall, reducing the actual intensity at the wall. Also, the Au foil was 1.5 mm from the aperture and 3.5 mm from the window; in the NIF targets those distances will be ≈2 mm and ≈8 mm, respectively.

2. Hohlraum Experiments

The radiation environment in a laser-driven hohlraum is different than that of an open-geometry planar-target laser plasma: the laser beams overlap and are tightly focused at the LEH and the plasma scale lengths are changed by the closed geometry. VISAR measurements were performed with hohlraum targets to investigate if they could cause window blanking or other deleterious effects.

For these tests, NIF-sized Au re-entrant cones were inserted into OMEGA-scale hohlraums (2.55 mm long, 1.6 mm in diameter with 1.2-mm laser entrance holes). The cones were 5 mm long and had an 11° opening angle (to accommodate the f/3 VISAR focal cone). The NIF tip has a 10-μm wall formed into a spherical shape that will be ultimately placed within ~200 μm of the spherical-ablator inside surface. That tip has a 260-μm-diam aperture through which shocks are viewed. Inside the shell the cone wall is 50 μm thick and the rest of the cone is 100-μm-thick Au. The hohlraums were empty: no gas fill, no LEH windows. Figure 117.4(a) shows three views of these targets.

(a)

(b)

(c)

Window test at $T_{\rm rad}$ = 180 eV without D_2
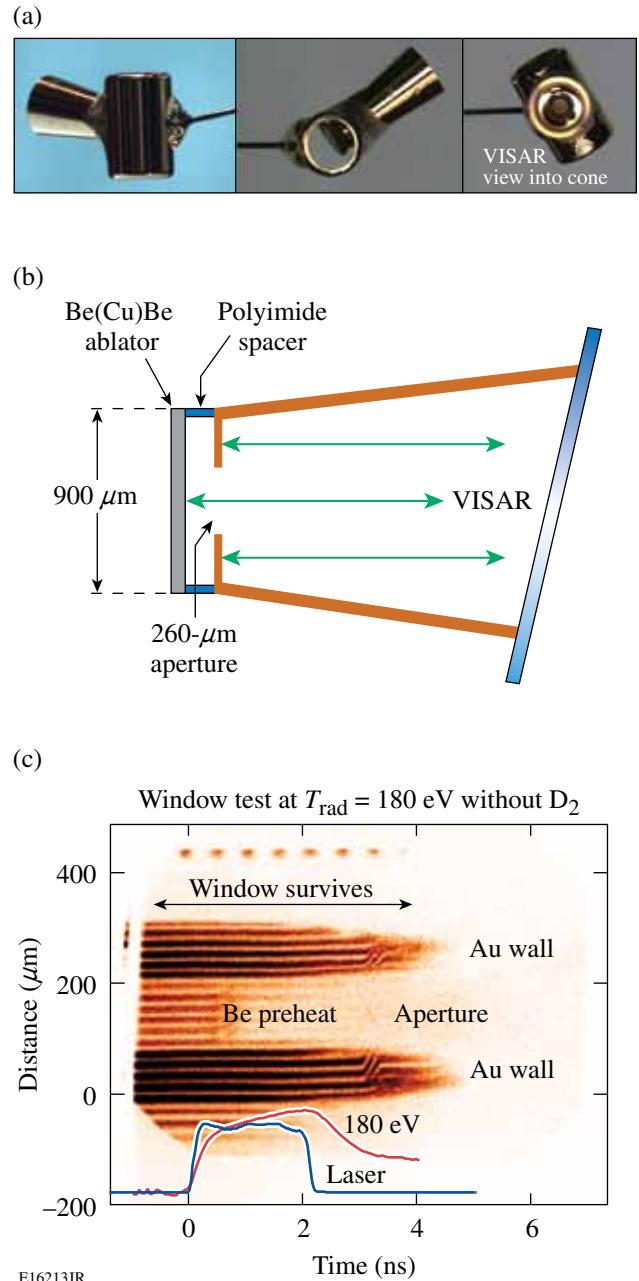
Figure 117.4

(a) The OMEGA targets have NIF-sized diagnostic cones inserted into the OMEGA scale-1 hohlraums. (b) The ablator and cone tip assembly for the OMEGA shock-timing tests in hohlraum targets. The Be−Cu sandwich replicates the opacity of a NIF ablator. (c) VISAR data for a warm, empty hohlraum heated to 180 eV. The probe beam reflects off the cone face and the ablator (through cone aperture). These data show the Be ablator unloading because of preheat and window transparency persisting throughout the experiment, thereby proving viability of this technique.

The OMEGA experiments used planar ablators, so those cones had a 10-μm-thick, 260-μm-aperture planar tip. The rest of the cone was identical to the NIF cone design. The ablators were sandwiches of Be and Cu to simulate the x-ray opacity of the Cu-doped Be ablators[2] for the NIF. They were comprised of two 75-μm Be foils with a 0.5-μm Cu foil in between and were "brazed" to form a glueless bond. The ablators were mounted 190 μm from the cone tip to replicate the shell-to-cone-tip distance in the NIF targets.

One concern was that M-band x rays entering the aperture at high angles could heat the inner cone wall sufficiently to create a secondary hohlraum that would re-radiate and blank the window. To mimic the spherical-capsule geometry, which allows these high-angle rays to enter the aperture, the ring that held the planar ablator away from the cone tip was made of 60-μm polyimide. This ring has similar opacity to the Be−Cu ablator. The ablator and cone geometry are shown in Fig. 117.4(b).

The VISAR diagnostic is not perpendicular to any convenient and symmetric hohlraum axes in the OMEGA chamber. Rather than perturb the irradiation pattern and line of sight for radiation-temperature measurements (Dante), the VISAR cones were inserted 79.2° from the hohlraum axis to accommodate this offset [Fig. 117.5(a)]. This deviation from the NIF geometry is considered conservative since, at this angle, the cone views the region irradiated by beams with lower angles of incidence and are, therefore, of higher intensity than those at the equator. The cones were inserted so the ablators were on the central axis of the hohlraum. The ablators were ~0.8 mm from the hohlraum wall, less than half the distance of the NIF targets to the hohlraum wall.

The hohlraums were irradiated by 38 OMEGA beams with no beam smoothing and having 2-ns-long, temporally square pulses to produce radiation temperatures of >180 eV. VISAR measurements of the rear side of the ablator (i.e., made through the window and cone aperture) are shown in Fig. 117.4(c). The VISAR data comprise a series of interferometer fringes[13,16] whose vertical position is proportional to the velocity of the reflecting surface (shock wave or ablator surface). Figure 117.4(c) shows two regions of the target probed by the VISAR: the inner surface of the aperture, and the rear surface of the ablator, viewed through the aperture. Prior to the drive pulse and subsequent thermal radiation (graphs shown in plot), the fringes are horizontal and of constant intensity. As the drive temperature rises, the ablator is heated and, at ~1 ns, the expanded rear-surface material absorbs the VISAR probe beam, causing the signal to diminish. It is important to

note that the signal from the Au aperture surface (above and below the ablator signal) that is well shielded and, therefore, not preheated and does not expand, persists throughout the drive pulse. This indicates that the window remains transparent and survives the radiation from the hohlraum.

Experiments with hohlraums driven to T_{rad} > 200 eV produced blanking in the quartz window. This is consistent with the open experiments described in **VISAR Windows** (p. 3) and

(a)

Quartz window

NIF-sized cone

D_2

VISAR

Be–Cu–Be ablator

(b) Successful cryogenic D_2 test

Au wall

Aperture

Shock in D_2

Drive laser

(c) SOP shot 48881

Shock in D_2

Emission from aperture edge

Shock breakout

Shock reaches aperture

E16219bJR
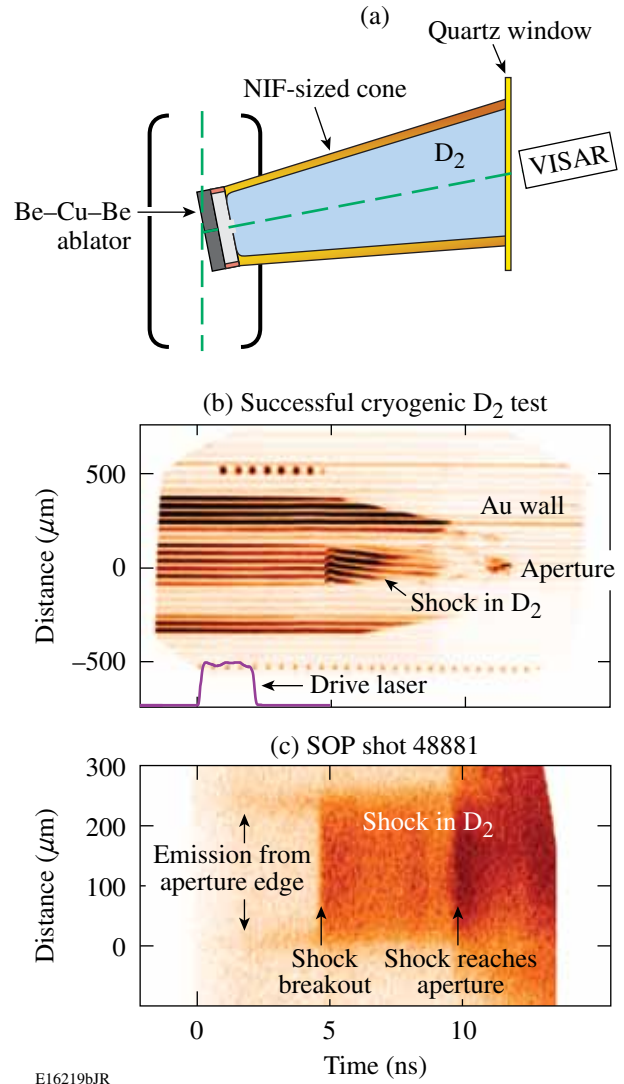
Figure 117.5
(a) The cryogenic target is identical to that in Fig. 117.4(a), except that the cone is filled with liquid deuterium and the assembly is mounted on a cryostat. (b) VISAR data show again that the window remains transparent and that the shock in deuterium is observed. (c) Streaked optical pyrometer (SOP) data showing temporal features (in self-emitted light) that confirm the behavior in the VISAR data (b).

ultimately limit the conditions under which windows can be used. In the **Fourth Shock Timing** section below a windowless target is proposed for timing the fourth "shock."

During these experiments it was found that scattered light from the incident drive beams could blank the VISAR window from the outside. To prevent this, the diagnostic cones were fitted with shields to block all scattered light from irradiating the window. This is an important aspect of the NIF target design because a significant amount of unconverted light passes within a 3- to 10-mm annulus around NIF targets. As a further precaution, some cones were coated on the inside with CH to minimize any secondary-hohlraum effect by reabsorbing any low-energy photons re-emitted by the cone wall upon irradiation by M-band emission. As expected, these experiments also showed no window blanking and CH overcoats are not expected to be required at the NIF.

3. Cryogenic Experiments

Experiments were performed using cryogenic targets filled with liquid deuterium. The hohlraums were empty while the cones were filled with liquid deuterium between the ablator and the VISAR window [Fig. 117.5(a)]. Figure 117.5(b) shows the VISAR data from such an experiment driven at 135 eV. These data clearly show that the window survives throughout the drive pulse and the shock in the deuterium is observed. The self-emission data [Fig. 117.5(c)] from the streaked optical pyrometer (SOP)[18] exhibit identical temporal features that confirm the timing of the shock breakout (arrival at rear surface) and arrival time at the aperture after transiting the ablator–cone gap. Additionally, the heating of the aperture edge, as evidenced by its self-emission, is seen early in time. While this heating is unavoidable, it is not expected to present a problem with the measurements or their precision.

These data at 135 eV confirm that the proposed shock-timing technique is viable for the NIF targets driven by higher radiation temperatures because the OMEGA experiments produce more M band than is expected on the NIF. Figure 117.6 shows the predicted M-band flux from the NIF experiments at 165 eV, compared to the OMEGA emission from the 135-eV hohlraums. Note that the OMEGA hohlraums produce significantly more x-ray flux above 2 keV than expected from the NIF targets. This is because the OMEGA hohlraums have a smaller fraction of wall irradiated by beams and have lower time-dependent albedo and, therefore, require a higher beam intensity to reach a given radiation temperature. This higher intensity leads to more M band, which is produced primarily in the laser-spot regions.
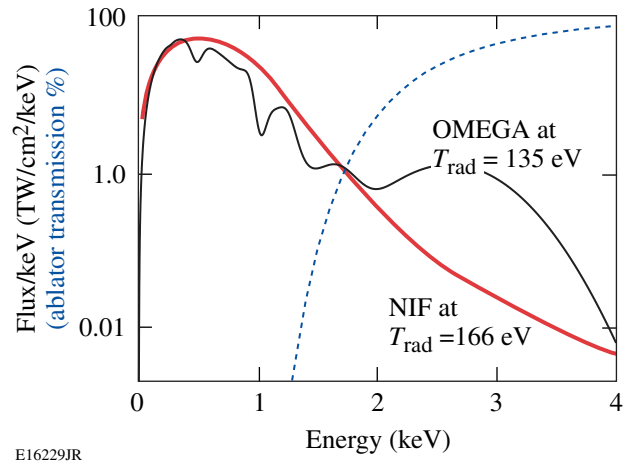
Figure 117.6
Radiation spectrum expected on the NIF (thick solid curve) for conditions of the third shock (165 eV) and that for the OMEGA experiments at 135 eV (thin solid curve). Note that above 2 keV, the OMEGA experiments have higher fluxes. The ablator transmits (dashed curve) this region of the spectrum.

4. Fourth Shock Timing

The tuning experiments for NIF shock timing must also time the compression wave (or fourth shock) that is driven by radiation temperatures above 250 eV. The fluxes from these drives are expected to blank the VISAR window; therefore, a windowless target was designed. These targets have a re-entrant cone with no aperture, confining the deuterium only to the capsule. The compression wave will be detected by the arrival of the shock at the inner surface of the cone tip. This will be detected as either movement or cessation of the fringes. If the released material remains solid when the shock arrives at a solid/vacuum interface, this material can continue to reflect the VISAR probe beam and the free surface velocity can be detected. If, however, the material is sufficiently heated to melt and then expand, it typically produces a density gradient that absorbs the probe beam at the rear surface and the signal then vanishes.

This concept was tested on OMEGA with the hohlraum driven to much higher temperatures. Figure 117.7(a) shows the target design that comprised a standard NIF cone and [in Fig. 117.7(b)] the Be–Cu–Be ablator sandwich. The cone tip had an Au step assembly (16 μm and 36 μm thick) facing the ablator. VISAR and SOP probed the rear surface of that assembly. In these experiments, for simplicity, there was no deuterium in the gap between the ablator and the Au step. The gap was filled with 1 atm of air during fabrication and well sealed. There was no need for a VISAR window, so none was used at the end of the cone. The VISAR data [Fig. 117.7(c)] show continuous

fringes until the arrival (at 3.5 and 4 ns) of shocks at the rear of the two steps.

The radiation temperature in this experiment was 220 eV, and as was the case seen in Fig. 117.6, the M-band emission was significantly (12×) higher than that expected for a 250-eV NIF hohlraum. As a result, the shock that first breaks out of the two steps was driven by the M-band emission incident on the cone face. The subsequent arrival of the shock driven by the thermal spectra is seen as a brief increase of intensity that occurs at the thin step [upper portion in Fig. 117.7(c)] at ~5.7 ns. These features are confirmed by 1-D simulations using the experimental drive including the M-band emission. Simulations
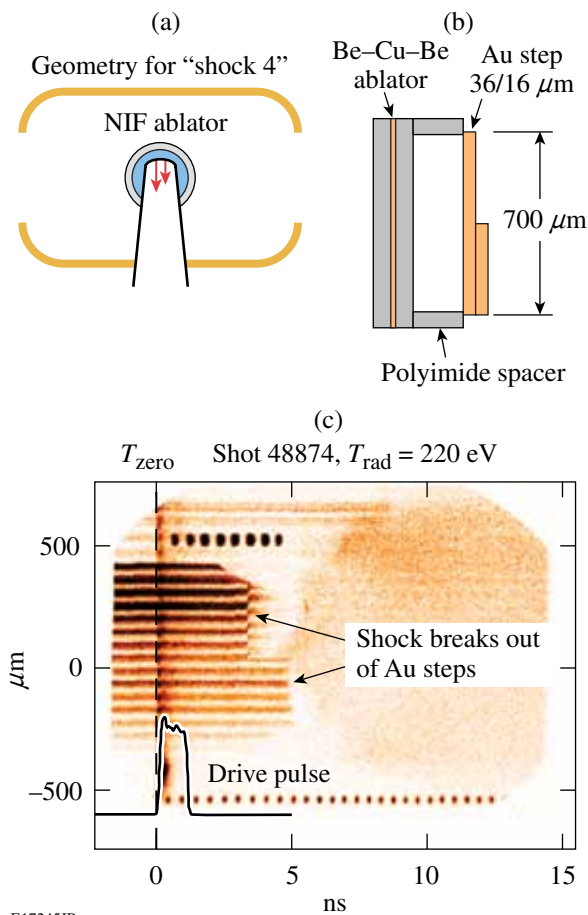
Figure 117.7
(a) The NIF target configuration used to measure the timing of the compression wave. It is similar to the design in Fig. 117.2, except there is no aperture in the cone and no diagnostic window. (b) The OMEGA cone-tip design used to test the compression-wave timing technique. (c) VISAR results for a target driven to 220 eV, showing persistence of VISAR fringes until shock breakout. This breakout provides an unambiguous arrival time for the shock at the rear surface of the steps.

of NIF targets predict that the thermal shock breaks out well before any M-band–driven shocks.

The unambiguous breakout feature is the cessation of the fringes caused by the release of material absorbing the VISAR laser. This is a common observation in shock experiments using opaque samples. This technique is applicable to shock experiments over a wide range of shock pressures. At lower pressures, the breakout may not cause a cessation of fringes but, instead, the onset of motion. At very high drive intensities, the sample could be preheated, causing the rear-surface release. In this latter case, the VISAR signal could be lost, but experiments show that the arrival of the shock can still be observed [as in Fig. 117.7(c)] because it steepens the density gradient, producing a brief reflected VISAR signal and an unambiguous SOP signal. [The steepening occurs in times less than the resolution time of the VISAR (30 ps) and lasts a few hundred picoseconds, depending on the time it takes for that material to relax and once again form an absorbing profile.] This provides confidence that this technique can be used for a wide range of conditions on the NIF. It is expected that the shock-propagation time across the cone tip can be accounted for with precision sufficient to achieve the necessary shock timing on the NIF.

5. Spherically Convergent Shock Experiments

Previous experiments used planar ablators and single drive pulses for expediency. The NIF experiments will involve multiple, spherically converging shocks—conditions not attainable in OMEGA hohlraum experiments without resorting to quarter-scale spherical targets with insufficient reflecting surface area. To study these effects, larger-scale, direct-drive experiments were performed on cryogenic spherical targets. These targets were 900-μm-diam, 10-μm-thick CD shells fitted with the NIF-scale VISAR cones. The assemblies were filled with liquid deuterium and irradiated by 36 OMEGA beams in the hemisphere centered on the VISAR line of sight [Fig. 117.8(a)]. This produces spherical shocks that converge toward the cone aperture. Figure 117.8(b) shows the VISAR record for an experiment driven by the multiple laser pulses shown at the base of this figure.

These targets have a 1000-Å Al coating on their outer surface. Before time zero, the VISAR probe beam reflects off the inner surface of this layer. At time zero, the laser ablates the layer and the x rays from the laser plasma cause the CD shell to blank (absorb) the VISAR probe beam, causing the VISAR fringes to disappear. At about 0.5 ns, the shock emerges from the CD shell and enters the deuterium. The VISAR fringes return because the shocked deuterium is reflective (>50%) and
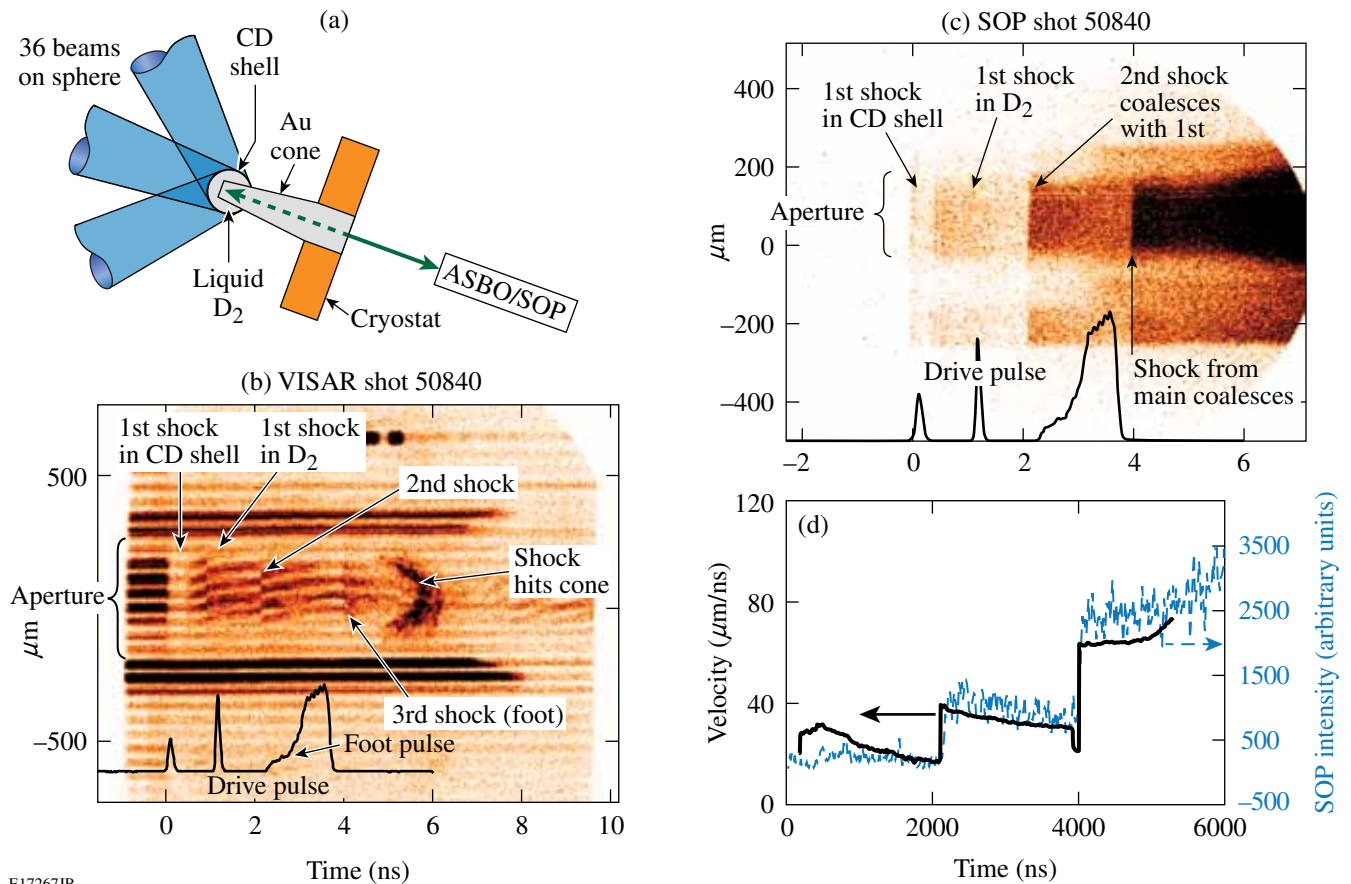
Figure 117.8

(a) Direct-drive cryogenic spherical targets used to study the timing of multiple convergent shocks on OMEGA. (b) VISAR record for three shocks in deuterium produced by the multiple pulses shown at the base of the figure. Evidence of shock coalescence (stronger shocks overtaking weaker ones) are evident at 2 and 4 ns; these indicate that multiple convergent shocks can be timed with this target and diagnostic configuration. (c) The SOP data show that the coalescence features observed in VISAR data are replicated in the self-emission intensity. (d) Shock velocities inferred from VISAR data and self-emission intensity histories for the data shown in (b) and (c).

the unshocked deuterium in front of it remains transparent. The curvature in the fringes from 0.5 to 2 ns results from deceleration of this first shock, which decays because it is unsupported: the first drive pulse has turned off. Just after 2 ns the shock produced by the second drive pulse (at 1.2 ns) overtakes the first shock. This is observed as a jump in fringe position produced by the jump to the new shock velocity. Since the first shock produces conduction electrons in the deuterium, the shocked material is reflective and opaque to the VISAR probe. As a result, VISAR cannot detect the second shock "through" the first shock, until the second overtakes the first shock.

At about 2.25 ns the "main" drive pulse begins at low intensity and ramps to higher intensity. At 4 ns, the shock from this pulse overtakes the combined first and second shocks, producing another jump in fringe position. About 1 ns later the

shock hits the front surface of the Au cone. The bright feature that begins at ~5 ns is either reflection off of or self-emission from the hot material from the aperture that was heated by the shock. This material flows into the aperture, producing the converging feature from 5 to 6 ns. Ultimately the material cools, the shock passes it, and the decaying shock can again be observed at late times. It should be noted that in the NIF tuning campaign the pertinent shock-timing events are over before the shock reaches the cone face.

The self-emission from the shock was acquired simultaneously with VISAR data. Figure 117.8(c) depicts the intensity of light (590 to 850 nm) emitted by the shock and detected by the SOP. The features of the three shocks described above are plainly visible in Fig. 117.8(c). The material closing into the aperture is not observed (as in the VISAR data), but the arrival

of the shock at the aperture can be seen as a spatial broadening of the emission region. The slope of this growing edge can be traced back to the original diameter, intersecting at ~5 ns, which is the arrival time observed by VISAR. Figure 117.8(d) shows the shock velocity (deduced from VISAR) and the self-emission intensity histories measured for this shot. Note that these measured velocities span the range of shock velocities (20 to 57 km/s) that are prescribed for the first three shocks in a NIF ignition target, demonstrating this technique at applicable shock conditions.

These data confirm that VISAR and SOP can readily detect the velocities and the timing of spherically converging shocks that have traveled (and converged) by the ~200-μm distance from the shell to the cone tip. The lateral extent of the VISAR data is governed by the amount of probe light that is returned into the collection lens of the diagnostic and is proportional to the curvature of the spherical shell. The NIF capsules will be about twice the size of those used for the OMEGA experiments, so the detected region will be twice that of the OMEGA experiments while the radial distance traveled is the same. The OMEGA conditions are therefore more stringent (i.e., smaller curvatures) than the NIF experiments.

Conclusions

The National Ignition Campaign requires that multiple spherically convergent shock waves be timed to high precision. Targets with re-entrant cones will make it possible for optical diagnostics to probe the interior of the capsules *in situ*, with minimal interference to the x-ray-flux environment driving the probed capsule region. These targets also make possible the precise optical measurements of the velocity profiles (and therefore timing) of multiple shocks in the harsh radiation environment of an ignition hohlraum; this presents formidable challenges.

Experiments were performed on the OMEGA laser to assess the viability of the proposed techniques. These experiments used open and hohlraum geometries to select quartz as the material for the diagnostic window in the NIF targets. Hohlraum experiments showed that quartz remains transparent throughout experiments that were driven to radiation temperatures greater than 180 eV, and that produced M-band emission greater than that expected on ignition targets, up to the timing of the third shock. Cryogenic experiments confirmed that the column of liquid deuterium is not adversely affected by thermal and M-band x rays from the hohlraum. Direct-drive experiments on cryogenic spherical targets demonstrated that shock timing can be performed on multiple, spherically

convergent shocks, and that shocks up to ~70 km/s can be detected optically.

Each of the OMEGA experiments had more adverse conditions than those expected on the NIF, i.e., higher M-band emission, less standoff distance to the window, and smaller radius of curvature. These experiments, therefore, provide high confidence that the NIC plan for shock timing is viable and will successfully time shocks to adequate precision for ignition targets.

REFERENCES

1. J. D. Lindl, *Inertial Confinement Fusion: The Quest for Ignition and Energy Gain Using Indirect Drive* (Springer-Verlag, New York, 1998), Chap. 6, pp. 61−82.

2. T. R. Dittrich *et al.*, Phys. Plasmas **6**, 2164 (1999).

3. B. A. Hammel *et al.*, Plasma Phys. Control. Fusion **48**, B497 (2006).

4. D. H. Munro *et al.*, Phys. Plasmas **8**, 2245 (2001).

5. D. H. Munro, H. F. Robey, B. K. Spears, and T. R. Boehly, Bull. Am. Phys. Soc. **51**, 105 (2006).

6. T. R. Boehly, D. L. Brown, R. S. Craxton, R. L. Keck, J. P. Knauer, J. H. Kelly, T. J. Kessler, S. A. Kumpan, S. J. Loucks, S. A. Letzring, F. J. Marshall, R. L. McCrory, S. F. B. Morse, W. Seka, J. M. Soures, and C. P. Verdon, Opt. Commun. **133**, 495 (1997).

7. S. W. Haan *et al.*, Eur. Phys. J. D **44**, 249 (2007).

8. S. W. Haan *et al.*, Phys. Plasmas **12**, 056316 (2005).

9. D. G. Hicks, T. R. Boehly, P. M. Celliers, J. H. Eggert, S. J. Moon, D. D. Meyerhofer, and G. W. Collins, Phys. Rev. B **79**, 014112 (2009).

10. P. M. Celliers *et al.*, Phys. Rev. Lett. **84**, 5564 (2000).

11. L. M. Barker and R. E. Hollenbach, J. Appl. Phys. **43**, 4669 (1972).

12. P. M. Celliers *et al.*, Appl. Phys. Lett. **73**, 1320 (1998).

13. P. M. Celliers, D. K. Bradley, G. W. Collins, D. G. Hicks, T. R. Boehly, and W. J. Armstrong, Rev. Sci. Instrum. **75**, 4916 (2004).

14. T. R. Boehly, T. J. B. Collins, O. Gotchev, T. J. Kessler, J. P. Knauer, T. C. Sangster, and D. D. Meyerhofer, J. Appl. Phys. **92**, 1212 (2002).

15. H. F. Robey, D. H. Munro, B. K. Spears, M. M. Marinak, O. S. Jones, M. V. Patel, S. W. Haan, J. D. Salmonson, O. L. Landen, T. R. Boehly, and A. Nikroo, J. Phys., Conf. Ser. **112**, 022078 (2008).

16. T. R. Boehly, E. Vianello, J. E. Miller, R. S. Craxton, T. J. B. Collins, V. N. Goncharov, I. V. Igumenshchev, D. D. Meyerhofer, D. G. Hicks, P. M. Celliers, and G. W. Collins, Phys. Plasmas **13**, 056303 (2006).

17. W. Theobald, J. E. Miller, T. R. Boehly, E. Vianello, D. D. Meyerhofer, T. C. Sangster, J. Eggert, and P. M. Celliers, Phys. Plasmas **13**, 122702 (2006).

18. J. E. Miller, T. R. Boehly, A. Melchior, D. D. Meyerhofer, P. M. Celliers, J. H. Eggert, D. G. Hicks, C. M. Sorce, J. A. Oertel, and P. M. Emmel, Rev. Sci. Instrum. **78**, 034903 (2007).